

Assessment of Nerve Regeneration through a Novel Microchannel Array

Benjamin Maimon^{1,2,*}, Anthony N. Zorzos^{1#}, Katherine Song^{1,3}, Rhyse Bendell⁴, Ron Riso¹ and Hugh Herr^{1,2}

¹MIT Media Lab, Center for Extreme Bionics, Massachusetts Institute of Technology, Cambridge, Massachusetts, USA

²Harvard-MIT program in Health Sciences and Technology (HST), Massachusetts Institute of Technology, Cambridge, Massachusetts, USA

³Department of Electrical Engineering and Computer Science, Massachusetts Institute of Technology, Cambridge, Massachusetts, USA

⁴Department of Mechanical Engineering, Massachusetts Institute of Technology, Cambridge, Massachusetts, USA

#These authors contributed equally to this work.

*Corresponding author: Benjamin Maimon, MIT Media Lab, Center for Extreme Bionics, Massachusetts Institute of Technology, Cambridge, Massachusetts, USA, Tel: 6172535960; E-mail: bmaimon@media.mit.edu

Received date: April 17, 2016; Accepted date: April 29, 2016; Published date: May 5, 2016

Copyright: © 2016 Maimon B, et al. This is an open-access article distributed under the terms of the Creative Commons Attribution License, which permits unrestricted use, distribution, and reproduction in any medium, provided the original author and source are credited.

Abstract

Advancements in robotic technologies have enabled a significant improvement in the clinical efficacy of prosthetic limbs for persons with upper and lower-extremity amputations. However, significant challenges still remain in establishing a biomimetic bidirectional neural communication between amputees and their external powered prostheses. Regenerative peripheral nerve interfaces may offer a high-resolution alternative to conventional nerve interface technologies for their unique potential to provide increased biospatial resolution for both the control of and feedback from an external powered prosthesis. Here, we present three separate designs for 3-D microchannel arrays, each having 16-20 channels measuring 200 μm by 200 μm : one passive (without integrated electrodes), one active (with integrated electrodes), and one active with a porous collagen scaffold. With the array positioned between proximal and distal nerve endings, we evaluate their effectiveness in tibial n. regeneration *in vivo* in both rats (N=4) and ferrets (N=4). Using immunofluorescence, we report robust mixed sensory and motor nerve regeneration through the microchannels in all rats, and weak regeneration in 2 of 4 ferrets, suggesting both interspecies regeneration variability and the lack of benefit of axially oriented collagen in improving ferret nerve regeneration through microchannels.

Keywords: Microchannels; Robotics; Electromyography; Limb; Nerves

Introduction

As wearable robotics has advanced in design and miniaturization, a large variety of advanced upper and lower-extremity prostheses have been built to improve the quality of life for persons with amputation (PWA). The commercially available bebionic3 is a myoelectric-controlled robotic device, capable of 14 different grip patterns that can enable a handshake, pick up a key, control a computer mouse, and perform a range of other tasks. However, because efferent control in the bebionic3 and other upper-extremity limb prostheses is limited to skin surface electromyography (EMG) of only 1-2 independent muscle bodies, the user has to manually switch between different grip patterns with either a co-contraction reset or a change of settings on the interface computer, limiting native intuitive control. New developments with implantable myoelectric sensors (IMES) have enabled recordings from a larger number of individual residual muscle bodies in both upper limb [1] and lower limb PWA [2]. However, residual muscle bodies vary from person to person – persons with transhumeral and transfemoral amputations lack the native residual muscle bodies of the forearm and leg respectively, which control motion in the wrist, hand, ankle and foot. To provide a higher degree of control, direct recordings from the nerves may be able to recreate the independent muscle signals lost during amputation, consistent with evidence suggesting the somatotopic arrangement of peripheral nerves [3,4].

Recently, several groups have developed neuroprosthetic interface devices capable of providing long-term touch and vibration feedback for PWA using nerve cuffs and intrafascicular electrodes [5,6]. These devices have enabled moderate to long-term afferent feedback to PWA from “second skin” pressure sensors located on the fingertips of the prosthesis; however, the neuroprosthetic interfaces employed are anatomically limited. Nerve cuffs can only selectively stimulate the external surface of large nerves and they cannot selectively stimulate a small, targeted bundle of axons within the body of the nerve [7]. Hook electrodes have increased spatial range by flattening the nerve, but, like cuff electrodes, they do not have high spatial resolution for groups of axons [7]. Intrafascicular electrodes have better spatial resolution in the body of the nerve, but they are limited to recording only a small fraction of nerve axons and may have long-term complications [7]. Implantable microarrays provide exquisite resolution, down to individual single-unit activity from individual sensory action potentials [8]; however, they are associated with significant pathology to the nerve due to high mechanical stiffness [7].

Regenerative microchannel peripheral nerve interfaces offer a highly selective, mechanically compliant alternative to conventional nerve interface technologies because of their unique potential to provide increased biospatial resolution for both control of and sensory feedback from a prosthesis [7]. Previous attempts to develop microchannel peripheral nerve interfaces have been met with some success [9-12]. Musick et al. implemented a rat sciatic nerve end-to-end repair model to demonstrate nerve regeneration within an uncoated poly dimethyl siloxane (PDMS) microchannel array [9]. The microchannel functioned to bridge the transected nerve, which grew through the

70 110 μm x 120 μm channels. Although regrowth was not present in all channels, each channel that exhibited regrowth contained blood vessels, myelinated nerves, and fibrous tissue. One key finding was that the total number of nerve fibers throughout all channels decreased significantly from 2067 ± 617 at 3 months postop to 442 ± 193 at 9 months postop, compared to an estimated $\sim 27,000$ axons in the healthy rat sciatic n [13]. Possible explanations include a pruning of axonal sprouts, chronic inflammatory response or mechanical compression causing axonal “centering” towards the middle of each channel. To mitigate against both chronic inflammatory response and mechanical compression, the Musick et al. study supports the idea that geometry of the channel may be of critical importance; small channel size may be a limiting factor in the development of healthy nerve fibers, due to a 15 μm -50 μm thick contractile capsule guiding nerve regeneration and outgrowth [14].

In addition to cross-sectional area, microchannel length has been previously analyzed for optimal regeneration. Using PDMS channels, Lacour et al. determined that a 1 mm length was the best to encourage proliferation based on total axon counts at 4 weeks and 12 weeks postop through the channel and that numbers dropped significantly when the channels were larger than 3 mm in length. Interestingly, the mean number of axons increased in the 1mm length channel, from 171 at 1 month postop to 1,427 after 3 months postop, likely due to the additional sprouting in the 2 month period [10]. Recently, in the study of Musick et al., active microchannels were implemented in a study that monitored long-term recordings from nerves over the gait cycle in awake moving animals [15]. Increased neural signals were differentially associated with the plantarflexion portion of the gait cycle, as would be expected with direct recordings from motor neurons. However, an analysis of motor neuron distribution within the channels may have helped explain whether channels exhibiting stronger electroneurographic signals during plantarflexion were directly associated with a high composition of large motor axons. The objective of this study is to evaluate nerve regeneration through three types of nerve arrays: passive, active, and active with collagen. The passive arrays we implant into the rat tibial n. and the active and active with collagen we implant into ferret tibial n. We employ electrophysiology and immunofluorescence to assess the extent of regeneration through these constructs, which enables the identification of unique populations of nerve subtypes by channels.

Methods

Passive microchannel fabrication

The passive microchannel array fabrication process utilized standard microfabrication and assembly techniques [10]. The final device design was a 4×4 array of 3 mm length, 200 μm wide square channels, with a pitch of 250 μm in both dimensions. The array was composed of layers of polydimethylsiloxane (PDMS), an elastomer commonly used in implantable biomedical devices, and in previous microchannel designs [9]. First, an SU-8 mold was photolithographically defined on a 4” silicon wafer substrate. A 200 μm thick layer of PDMS (Sylgard 184, Dow Corning, 10:1 mixing ratio) was spin-coated onto the mold and thermally cured. The individual layers were manually cut from the substrate and released from the mold. The full array was formed by manually stacking, aligning, and bonding individual PDMS layers using oxygen plasma techniques [16].

Active microchannel electrode array fabrication

The active microchannel arrays were fabricated from an SU-8 substrate, a flexible photosensitive polymer commonly used in the microelectronics industry because of its versatility and potential for generating high aspect-ratio structures [17]. As a biocompatible polymer [18,19] SU-8 has been extensively explored and used as an implant material for biomedical devices [20]. It was employed to fabricate our microchannel arrays, balancing functionality, scalability, and ease-of-use. The final device design in this study was a 4×5 array of 3 mm long, 200 μm wide square channels, with a sidewall thickness of 10 μm in both dimensions (Figure 1a). Each channel was embedded with three electrodes, one in the center and the remaining two on the outermost regions in a standard tripolar layout configuration for recording peripheral nerves [21].

The array comprised stacked individual layers, assembled in a 3-D format after planar fabrication was complete. First, a sacrificial release layer of aluminum was deposited onto a 6” silicon wafer. A 10 μm layer of SU-8 was photolithographically patterned on top of the aluminum, defining the device lower substrate. Then, titanium and platinum (10 nm and 50 nm, respectively) were patterned using a standard liftoff procedure [22], thereby defining the electrode sites, bond pads, and interconnects. A 2 μm thick SU-8 electrical insulation layer was patterned on top of the metal such that only the electrode sites and bond pads were exposed. The sidewalls of the microchannels were defined by patterning a 200 μm thick layer of SU-8. The sidewalls measured 10 μm wide and 3 mm long. Finally, the individual layers were released from the wafer by selectively etching the sacrificial aluminum layer.

The full array was formed by manually stacking, aligning, and bonding individual device layers. This was accomplished by using SU-8 itself as an adhesion layer. Several microns were deposited on the underside of each layer, via aerosol (SU-8 MicroSpray, Microchem), and the layers were manually stacked, aligned, and bonded (Figure 1a). The bonding procedure was the same as standard SU-8 curing methods, utilizing UV-exposure and thermal treatment.

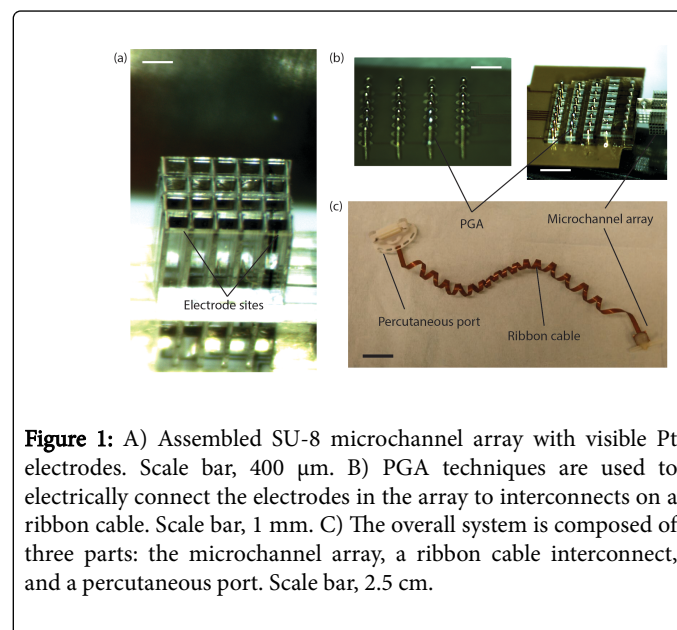


Figure 1: A) Assembled SU-8 microchannel array with visible Pt electrodes. Scale bar, 400 μm . B) PGA techniques are used to electrically connect the electrodes in the array to interconnects on a ribbon cable. Scale bar, 1 mm. C) The overall system is composed of three parts: the microchannel array, a ribbon cable interconnect, and a percutaneous port. Scale bar, 2.5 cm.

Each electrode in the array was electrically connected, via metallic traces integrated into a ribbon cable, to external recording and stimulating electronics. The ribbon cable was fabricated using standard flexible circuit board techniques, and was composed of a dual layer of copper traces embedded in polyimide, another commonly employed flexible biocompatible polymer [20]. Both terminals of the ribbon cable contained 2-D arrays of through-holes designed to interface with both the microchannel array and a percutaneous port. The ribbon cable was twisted into a helical shape under mild heat to allow for stretchability along its length. This manipulation was performed as a strain relief measure to provide relative movement buffer between the device and the percutaneous port to eliminate both buckling in the cable or transmission of mechanical force on the device.

The percutaneous port was composed of an electrical connector (NanoStrip, Omnetics Connector Corporation) embedded in a biocompatible shell. This shell was fabricated with a USP-VI biocompatible 3D printing resin (Duraform PA, 3D systems) and designed to allow for easy electrical docking and connection to skin tissue. The metallic tails of the electrical connector were connected to the through-holes of the ribbon cable using a biocompatible conductive epoxy (EP3HTSMed, Master Bond Inc). The interface was embedded in silicone. The microchannel array was connected to the ribbon cable using pin-grid array (PGA) techniques [23]. Individual gold-coated pins were connected to the array of through-holes in the ribbon cable, and that array of pins subsequently connected to the microchannel array bond pads (Figure 1b). All connections were again made through the use of a biocompatible conductive epoxy and the

interface was embedded in silicone. The final device measured ~20 cm long, but could be stretched more than 50% without significant force transmission (Figure 1c).

Collagen scaffold array fabrication

It was hypothesized that a porous collagen scaffold introduced within the microchannels may help enhance regenerated axon counts both in the short-term and long-term and help mitigate against the chronic foreign body response. To make the Collagen-GAG suspension for the channels, lyophilized bovine type 1 collagen (Advanced BioMatrix) was blended using a dispersing tool (IKA) with chondroitin 6-sulfate solution (C-4384, Sigma) in glacial acetic acid in a procedure previously described [24]. Each silicone tube end of the completed microchannel was sealed using cut micropipette tips sealed by a custom-fabricated elastomeric cylinder (Qure Medical). The blended collagen mixture was injected through the elastomer and into the microchannels using a 3 mL syringe and a 22G needle. A 25G needle was placed through the elastomer on the opposite side of the channel to permit air to flow out of the sealed channels. The filled Collagen-GAG device was slowly lowered at 100 $\mu\text{m/s}$ using a custom fabricated motor system into Slytherm XLT Heat Transfer Fluid (Chempoint) cooled to -100°C to axially orient ice crystals within the collagen [25]. Following the freezing, micropipette tips were quickly removed and the still-frozen device was rapidly transferred to a lyophilizer to be freeze-dried. Verification of the collagen matrix through the channels was performed with light microscopy (Figures 2a and 2b).

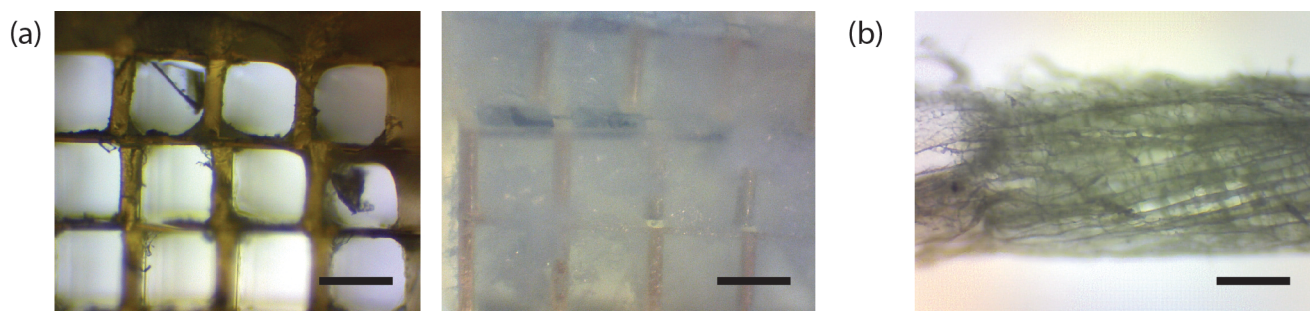


Figure 2: A) Micrograph of microchannel array cross section showing channels without and with an embedded collagen matrix. Scale bar, 200 μm . B) Micrograph of matrix removed from an individual channel showing axial orientation of porous collagen fibers. Scale bar, 40 μm .

EMG and histological analysis of passive array in rats

Experiments were conducted on four adult male Lewis rats under the supervision of the Committee on Animal Care at Massachusetts Institute of Technology. Under isoflurane anesthesia, a 1.5 cm skin incision was opened along the lateral aspect of the right hindlimb. The biceps femoris (BF) muscle was identified and detached from its insertion at the proximal tibia and reflected dorsocaudally. The tibial n. was identified electrically with a Checkpoint neurostimulator (Checkpoint Surgical) and transected 1 cm distal to the sciatic bifurcation. A fascicular dissection was performed on the sural n. proximal to the transection of the tibial n. The microchannel was sterilized with ethylene oxide before it was sutured to the tibial n. at both proximal and distal transection ends with 9-0 nylon suture. The BF muscle was reattached and the skin incision was closed with suture and wound glue. Following 5 months of regeneration, a 2 cm skin incision was made on the lateral aspect of the right hindlimb and the

microchannel was identified in the same surgical method described above. The sciatic n. proximal to the channel was identified, and a hook electrode was carefully wrapped around the nerve to elevate it from the surrounding tissue. Stimulation current was ramped until supramaximal stimulation was achieved, as measured by EMG. The current pulses delivered to the sciatic n. were 50 μs long and varied in amplitude from 0.01 mA to 1 mA.

To record EMG, a 36AWG stainless steel multifilament wire was threaded through 25G needles; the distal 2 mm was stripped of insulation and bent over the edge of the needle. Two wires were placed in each muscle by inserting and then removing the needle from two locations in the muscle body, located roughly 1 cm apart longitudinally. EMG recordings were amplified (a fixed gain of 200x) using the RHA2216 amplifier circuit (Intan Technologies), and wired to a Raspberry Pi (Premier Farnell) with custom-built software for recording and processing EMG. Data analysis was performed using

Matlab (Mathworks). Tissue specimens were fixed in 4% paraformaldehyde in 0.1 M Phosphate Buffer Solution (PBS) at 4°C overnight and were transferred to 70% ethanol for dehydration before subsequent paraffin processing. Under a dissecting scope, PDMS layers and platinum traces were meticulously peeled away from the paraffin-processed tissue samples between layers using Number 5 forceps (Fine Science Tools) as it was discovered that the soft PDMS prevented proper tissue sectioning. The remaining tissue was embedded in paraffin blocks and 10µm sections were cut every ~100 µm in the tissue through the block. Gel-coated slides (Leica) with the tissue slices were heated at 100°C for 30 minutes to induce epitope retrieval. Slides were then processed for immunofluorescence using primary antibodies anti-Neurofilament 200 (NF200) (Millipore, MAB1623) and anti-Choline acetyl transferase (CHAT) (Millipore, AB144P); secondary antibodies included Alexa Fluor anti-goat 568 nm (Life Technologies), Alexa Fluor anti-mouse 488 nm (Life Technologies), and DAPI. Slides were coverslipped in mounting medium (Dako) and images were captured with an Evos FL microscope.

EMG and histological analysis of active array in ferrets

Four adult ferrets (Charles River Labs) were anesthetized with intramuscular injections of ketamine/xylazine, followed by intubation and delivery of isoflurane anesthesia under supervision from the Committee on Animal Care at Massachusetts Institute of Technology. Ferrets were chosen for their large size, quadrupedal gait, and ability to withstand the large surgical procedure required. A 6 cm incision was made through the skin and connective fascia superficial to the distal femur, knee, and proximal tibia on the lateral aspect of the right lower limb. The BF muscle was identified, removed from its insertion at the proximal tibia, and reflected dorsocaudal to reveal the sciatic, tibial and peroneal nerves (Figure 3a).

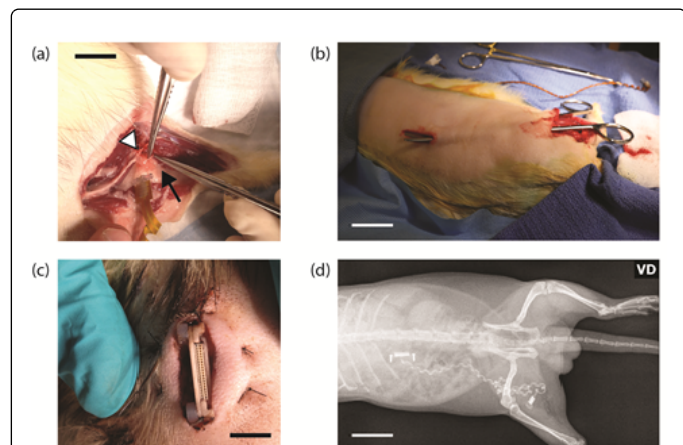


Figure 3: A) Distribution of sciatic n. branches in ferret with peroneal n. (arrowhead) and sural n. (arrow) dissected from tibial n. (forceps). Scale bar, 6 mm. B) Subcutaneous tunneling using shears from percutaneous port incision site (left) to microchannel implant site (right) with coiled ribbon cable in background. Scale bar, 3 cm. C) Percutaneous port with 40 pin connector sutured in subcutaneous space. Scale bar, 8 mm. D) Radiograph taken 1 week post-implant showing locations of channel adjacent to GN muscle and port adjacent to right caudal rib. Scale bar 3 cm.

A second ~3 cm incision was made through the skin at the ferret's ipsilateral dorsal surface, superficial to the 8th rib roughly 15 cm from

the first incision. Using a hemostat, the percutaneous port along with the coiled ribbon cable was tunneled through the subcutaneous fascia from the leg to the dorsal surface incision and was affixed at this incision using 5-0 nylon suture (Figures 3b and 3c). The sural n. was dissected proximally from the tibial n. enabling transection of tibial n. without sural sensory loss (Figure 3a).

The two silicone tubes terminating the microchannel on each end were sutured to the epineurium of the proximal and distal ends of the transected tibial n. using 9-0 Vicryl suture. Four ferrets were implanted with the synthetic SU-8 array: two with channels embedded with collagen and two without. The BF muscle was reattached distally over the channels, and the skin incision closed with suture and wound glue. One week following the operation, x-rays were taken to verify position and orientation of the device (Figure 3d).

Results

Passive microchannel in rats

In vivo regeneration was assessed 5 months after device implantation via wire EMG recordings from the (GN) and (TA) muscles in the anesthetized rat (Figure 4a). Current-controlled single pulses or pulse trains were applied to the sciatic n. proximal to its bifurcation into the tibial n. and peroneal n. using a custom-built hook electrode. Both electromyography (EMG) and ankle angular position was recorded in the leg. Direct stimulation of the sciatic n. resulted in ankle dorsiflexion, with corresponding EMG activity in both the TA and the GN for both single pulses and pulse trains at maximum voltage of ~10_mVpp prior to gain (Figure 4b). To verify electrophysiological regeneration through the microchannels, the peroneal n. and tibial n. branches around the microchannel were transected, and stimulation was reapplied at the sciatic n.

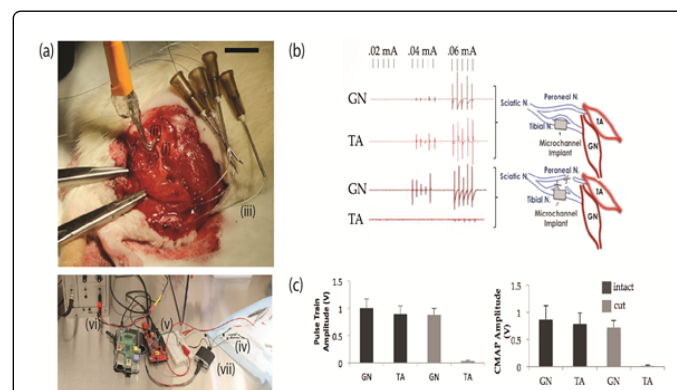


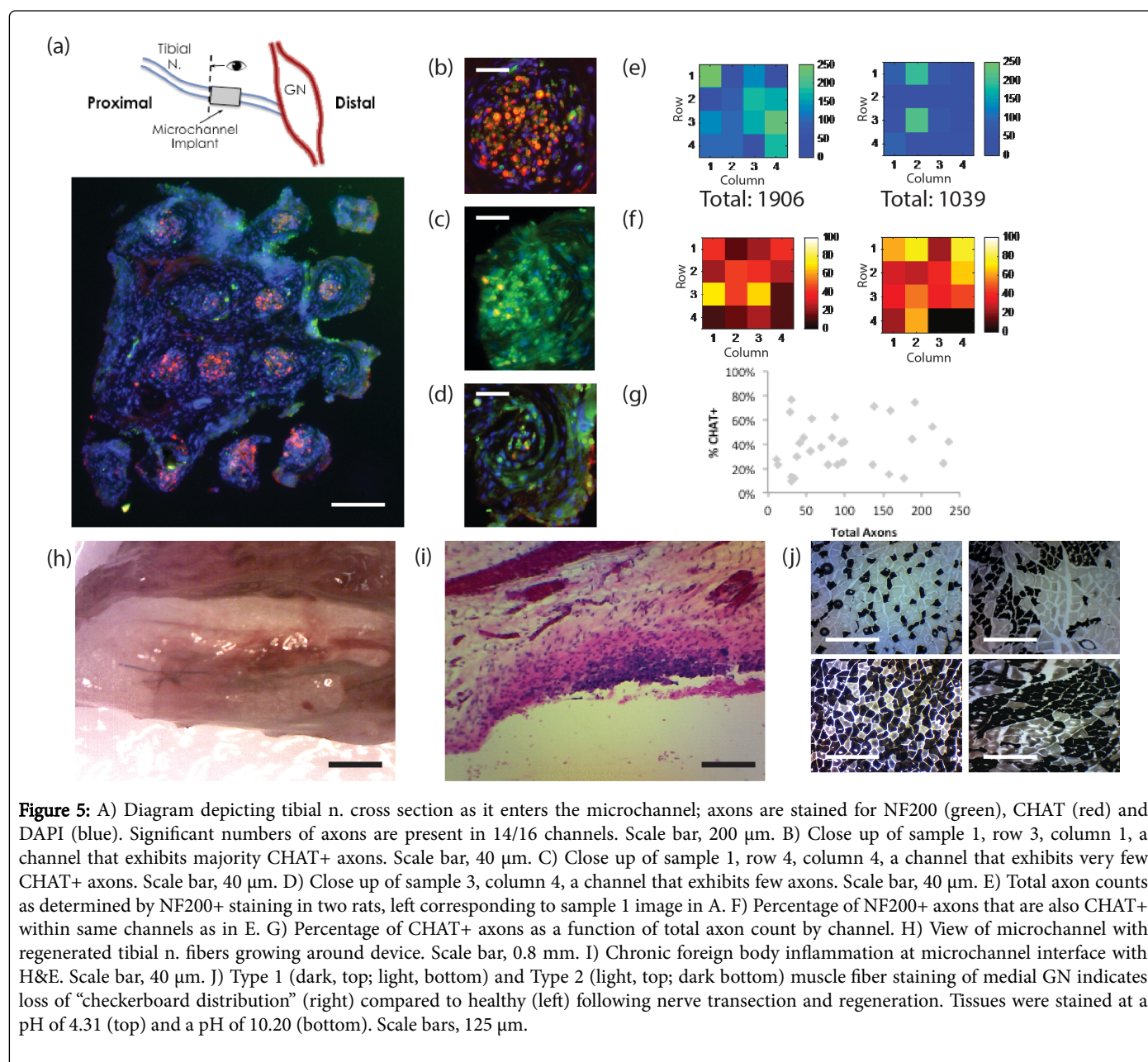
Figure 4: EMG recording equipment set-up for stimulating nerves and measuring downstream muscle activity. Sciatic n. (i), bipolar hook electrode(ii), TA/GN electrodes (iii), fine wire electrodes(iv), pulse generator (v), current source (vi), and amplifier / analog to digital converter (vii) shown. Scale bar, 1.5 cm. B) EMG traces showing electrophysiological activity in the GN through the microchannel, whereas the TA has lost activity. C) EMG pulse train voltage peak-peak amplitude and CMAP amplitude averaged from 5 and 15 trials respectively at supramaximal current stimulation of sciatic n.

Significant compound muscle action potential (CMAP) and EMG activity remained in the GN indicating tibial n. regeneration through

the PDMS channels, but a sharp drop of EMG activity was observed at the TA because its innervation pathway was cut (Figure 4c). For both individual pulses and pulse trains, maximum CMAP amplitude decreased in the GN after the fibers around the microchannel were transected ($P=0.02$, & 0.05 respectively by Student's t test), indicating that they too likely contributed to innervation of the GN. Mild plantarflexion was observed at the ankle, consistent with the GN^+/TA^- EMG response.

The sciatic n., TA, GN, tibial n., and microchannel were harvested for histological analysis. To assess for axon variation across individual channels by molecular subtype, double immunofluorescence of samples was conducted with anti-NF200 to stain for individual axons, anti-CHAT to stain for cholinergic motor axons [26,27], and DAPI, to assess for fiber distribution by channel post-regeneration (Figure 5a). Certain channels exhibited predispositions to CHAT+ fibers (Figure

5b), CHAT- fibers (Figure 5c), or low axon counts altogether (Figure 5d). The significant variation in total axon counts by channel as identified by individual NF200+ fibers ranged from a minimum of 13 axons per channel to a maximum of 236 axons per channel (Figure 5e). Significant variation in motor axon counts by channel as identified by CHAT+ fibers ranged from a minimum of 3 axons per channel to a maximum of 142 axons per channel, represented as a percentage of total fibers (Figure 5f). Certain channels exhibited a predisposition to either motor or sensory channels, in accordance with the "like-fibers" travel together hypothesis. However, it is unclear what geometric or biochemical factors contributed to this phenomena as there does not seem to be a strong relationship between either channel location within the array (Figure 5f) or total axon count within a given channel and the percentage of CHAT+ fibers within that channel (Figure 5g).



In the PDMS device, 200 μm channels were implemented in the attempt to overcome the 15-35 μm thick layer of connective tissue encapsulation of growing axons [14]. Increasing the channel size in this study to 200 μm over previously published work of \sim 110 μm channels [9] did not show a significant increase in axon counts either in individual channels (significant variation, but with maximum of \sim 250 axons) or total counts (2067 at 110 μm in sciatic n. in previous study vs. 1906 at 200 μm in tibial n. in current study). Nor did the larger channels prevent tibial n. fibers from simultaneously regenerating around the device (Figure 5h). It was discovered that fibrous nerve encapsulation was thicker within the 200 μm regenerating microchannels presented here than the previously published work on \sim 100 μm channels [9], possibly indicating a geometry-independent process for chronic inflammatory changes of a foreign body response or mechanical pressure response (Figure 5i), which built up over the 5 month regeneration period. To confirm regeneration in the GN, medial muscle fibers were evaluated enzymatically for activity using an ATPase stain to identify Type 1 and Type 2 muscle fibers [28]; fibers exhibited the characteristic loss of “checkerboard” pattern of Type 1 and Type 2 muscle fibers, as expected with nerve transection and regeneration (Figure 5j) [29].

Active microchannel electrode array in ferrets

Four months after implantation, ferrets were anesthetized and the lower limb was opened as described above; the tibial n. was stimulated with a 17 Hz, 0.5 mA, 50 μs PW stimulation pulse train, while monitoring for plantarflexion. The tibial n. was found to have regenerated in all of the ferrets, with stimulation of the proximal tibial n. producing a plantarflexion response. To evaluate regeneration through the microchannel device, all branches of the tibial n. regenerated around the microchannel, the sciatic n. and peroneal n. were cut, such that nerve activity was restricted to the device itself. In two animals (one of each the synthetic and hybrid-collagen designs), stimulation of sciatic n. produced a plantarflexion response. In both of these ferrets, the nerve did not appear to be growing through the majority of the channels, in contrast to the aforementioned rat experiments. Instead, regeneration was limited to a few channels of the array (Figures 6a and 6b). In the other two ferrets, a significant neuroma formed at the proximal end of the microchannel and all regeneration from the neuroma bypassed the device (Figure 6c).

Both stimulation and recordings through the percutaneous port were plagued by mechanical defects in the ribbon coil, likely caused by repeated animal movement that resulted in loss of electrical connectivity; to compensate for this loss, the ribbon cables were carefully delaminated during surgery and electrical current was applied directly to the platinum traces (Figure 6d). This resulted in plantarflexion in the same two of four ferrets which exhibited regeneration through the channels, demonstrating electrical connectivity to nerves growing through the device. The implant and all connected nerves were removed post-surgically. They were subsequently analysed microscopically and with immunofluorescence. It was found that the regenerated nerve in both tissues only grew through 1-2 of the channels in both animals (Figure 6e). The nerve tip exhibited the characteristic contraction closure response, indicating that regeneration had yet to be complete at 4 months; follow-up experiments in ferrets may require 6-12 months to restore full function. Cross-sections of the tissue were stained against NF200 and DAPI. The NF200+ neural tissue appeared to be growing in sparse and disorganized clumps with indiscernible individual axons (Figure 6f) possibly indicating immature neural tissue.

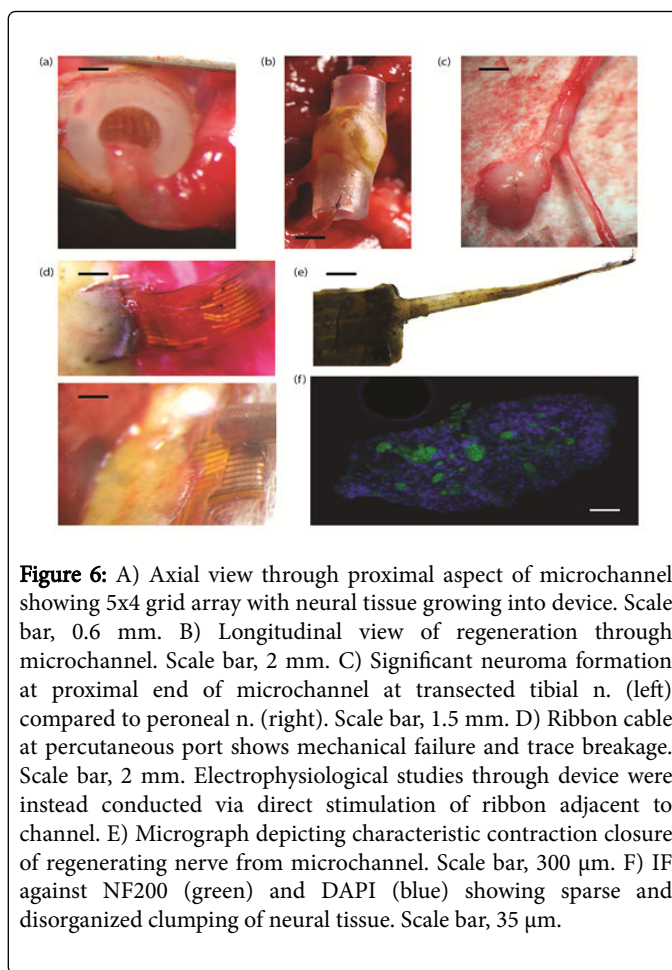


Figure 6: A) Axial view through proximal aspect of microchannel showing 5x4 grid array with neural tissue growing into device. Scale bar, 0.6 mm. B) Longitudinal view of regeneration through microchannel. Scale bar, 2 mm. C) Significant neuroma formation at proximal end of microchannel at transected tibial n. (left) compared to peroneal n. (right). Scale bar, 1.5 mm. D) Ribbon cable at percutaneous port shows mechanical failure and trace breakage. Scale bar, 2 mm. Electrophysiological studies through device were instead conducted via direct stimulation of ribbon adjacent to channel. E) Micrograph depicting characteristic contraction closure of regenerating nerve from microchannel. Scale bar, 300 μm . F) IF against NF200 (green) and DAPI (blue) showing sparse and disorganized clumping of neural tissue. Scale bar, 35 μm .

Discussion

In this paper, we present a new geometry for a passive PDMS microchannel and a novel design for an active regenerative microchannel electrode with and without a porous collagen scaffold; we employ these devices in rat and ferret animal models to analyze the extent of functional regeneration through the device by axon subtype. Despite robust EMG activity in both the GN and TA muscles, the strong dorsiflexion measured during electrical stimulation indicates a significantly weaker tibial n. to GN complex compared to the peroneal n. to TA complex: in a healthy animal, supramaximal sciatic stimulation results in co-contraction with predominant plantarflexion [30]. The dorsiflexion we observe could be attributed to either a weakened tibial n. or GN response. Possible explanations include the disorganized growth of fibers both outside and within the different channels interfering with the timing of end plate depolarization, incomplete myelination of the alpha motor fibers, which can take more than 20 months [31], decreased axon counts compared to the healthy tibial n. [13] or smaller diameter fibers [31]. Although the GN was not visually or histologically atrophied, muscle denervation and repair shown in the loss of checkerboard pattern distribution of Type 1 and Type 2 muscle fibers, is also independently associated with muscle weakness, especially in the early phases of regeneration [32]. Further work is needed to determine the precise cause of the weakened plantarflexor response noted through tibial n. channels.

The mixed distribution of motor and sensory fibers by channel provides insight into the way in which nerve fibers regenerate through microchannels. Whereas in the native nerve, alpha motor neurons projecting to the same muscle tend to travel together and sensory fibers within the nerve tend to travel together, there appears to be a loss of organization within the regenerating channels [27,33]. Although there appears to be a relationship between larger axon diameters and CHAT+ fibers, there does not appear to be a relationship between larger number of fibers and type of fibers within each channel. Previous research has shown in the setting of transection and restricted growth, large motor neurons tend to regenerate more quickly than small, less-myelinated sensory fibers [34], although research is conflicted, suggesting equal regeneration times for large myelinated sensory fibers [35]. It is possible that the differential speed of regeneration and subsequent pruning of the motor sprouts results in the predominance of mixed motor-sensory fibers within a channel at first; the sensory or motor fibers may be pruned at a later point in order to establish a greater segregation of axon subtype by channel in accordance with the normal physiological somatotropic and topographical distribution of healthy nerves [4]. Previous work suggests large alphas motor fibers may have more limited regeneration than large sensory fibers through a polyimide sieve [36]. Future work defining molecular subtypes and anatomic variation via retrograde tracers at unique post-transection time points may help elucidate the precise mechanisms underlying subtype segregation within channels during regeneration.

Many challenges remain to future adoption of microchannel nerve interface. These broad categories include 1) navigating both the wound contraction closure immune response as well as the chronic foreign body immune response, 2) electrically teasing nerve firings in the microvolt range, given a low signal-to-noise ratio for recording in awake, moving animals, and, 3) building a robust percutaneous system that addresses key areas for electrical and mechanical improvement in the device design. The difficulty of mitigating the inflammatory changes of the immune system is exemplified by thick fibrous encapsulation of regenerating axons where they make contact with the device. Axons are pushed to the center of each channel and surrounded by a ring of fibrous tissue. Possible explanations for this thick fibrous layer include foreign body response, but also include the direct mechanical transmission of force directly onto the surface of the nerve. To mitigate both, soft biocompatible flexible interfaces have long shown long-term advantages in peripheral nerve interfacing over rigid silicon-based sieve electrodes [37]; however, future work developing heavily biomaterial-based nerve interfaces is likely necessary before microchannel interfaces are robust enough to be used clinically. In all animals, a pathological neuroma formed at the proximal end of the transected tibial n. to some degree, indicating the nerve is still interpreting the microchannel as an obstructive mechanical impediment to regeneration. Future work includes *in vivo* ferret recording and stimulation of neural tissue, the development of a new histological method for evaluating soft bio-synthetic interfaces, and the replacement of the ribbon connector cable with coiled silicone insulating wires to promote the transmission of signals and stimulation to and from the nerve.

Acknowledgements

We would like to thank Jean-Francois Duval and Lillian Chen for their help with the electrophysiology work, Dr. Matt Carty and Dr. Simon Talbot at Brigham and Women's Hospital for their significant

help with the device implantation, the Koch Histology Core including Kathleen Cormier, Charlene Condon, Mike Brown for help with histology preparation, the Koch Microscopy Core including Jeff Wyckoff and Christopher Lee for help with microscopy and imaging, Dr. Ioannis Yannas, and Alex Springer for assistance with collagen preparation and lyophilization, the Microfabrication Technology Lab (MTL) at MIT for device construction, and Katharina Ross for assistance with muscle staining.

References

1. Pasquina PF, Evangelista M, Carvalho AJ, Lockhart J, Griffin S, et al. (2015) First-in-man demonstration of a fully implanted myoelectric sensors system to control an advanced electromechanical prosthetic hand. *J Neurosci Methods* 244: 85-93.
2. Össur Introduces First Mind-Controlled Bionic Prosthetic Lower Limbs for Amputees (2016) Össur Australia.
3. Dhillon GS, Lawrence SM, Hutchinson DT, Horch KW (2004) Residual function in peripheral nerve stumps of amputees: implications for neural control of artificial limbs. *J Hand Surg Am* 29: 605-615.
4. Badia J, Pascual-Font A, Vivó M, Udina E, Navarro X (2010) Topographical distribution of motor fascicles in the sciatic-tibial nerve of the rat. *Muscle Nerve* 42: 192-201.
5. Raspopovic S, Capogrosso M, Petrini FM, Bonizzato M, Rigosa J, et al. (2014) Restoring natural sensory feedback in real-time bidirectional hand prostheses. *Sci Transl Med* 6: 222ra19.
6. Tan DW, Schiefer MA, Keith MW, Anderson JR, Tyler J, et al. (2014) A neural interface provides long-term stable natural touch perception. *Sci Transl Med* 6: 257ra138.
7. Navarro X, Krueger TB, Lago N, Micera S, Stieglitz T, et al. (2005) A critical review of interfaces with the peripheral nervous system for the control of neuroprostheses and hybrid bionic systems. *J Peripher Nerv Syst* 10: 229-258.
8. Branner A, Normann RA (2000) A multielectrode array for intrafascicular recording and stimulation in sciatic nerve of cats. *Brain Res Bull* 51: 293-306.
9. Musick KM, Chew DJ, Fawcett JW, Lacour SP (2013) PDMS microchannel regenerative peripheral nerve interface. 6th International IEEE/EMBS Conference on Neural Engineering (NER).
10. Lacour SP, Fitzgerald JJ, Lago N, Tarte E, McMahon S, et al. (2009) Long micro-channel electrode arrays: a novel type of regenerative peripheral nerve interface. *IEEE Trans Neural Syst Rehabil Eng* 17: 454-460.
11. Srinivasan A, Guo L, Bellamkonda RV (2011) Regenerative microchannel electrode array for peripheral nerve interfacing. 5th International IEEE/EMBS Conference on Neural Engineering pp. 253-256.
12. Lancashire HT, Vanhoestenbergh A, Pendegrass CJ, Ajam YA, Magee E, et al. (2016) Microchannel neural interface manufacture by stacking silicone and metal foil laminae. *J Neural Eng* 13: 034001.
13. Schmalbruch H (1986) Fiber composition of the rat sciatic nerve. *Anat Rec* 215: 71-81.
14. Chamberlain LJ, Yannas IV, Hsu HP, Spector M (2000) Connective tissue response to tubular implants for peripheral nerve regeneration: the role of myofibroblasts. *J Comp Neurol* 417: 415-430.
15. Musick KM, Rigosa J, Narasimhan S, Wurth S (2015) Chronic multichannel neural recordings from soft regenerative microchannel electrodes during gait. *Sci Rep* 5: 14363.
16. Xiong L, Chen P, Zhou Q (2014) Adhesion promotion between PDMS and glass by oxygen plasma pre-treatment. *J Adhes Sci Technol* 28: 1046-1054.
17. Wang C, Cho SJ, Kim NY (2013) SU-8-Based Structural Material for Microelectronic Processing Applications.
18. Vernekar VN, Cullen DK, Fogleman N, Choi Y, Garcia AJ, et al. (2009) SU-8 2000 rendered cytocompatible for neuronal bioMEMS applications. *J Biomed Mater Res A* 89: 138-151.

19. Wang C, Cho SJ, Kim NY (2013) SU-8-Based Structural Material for Microelectronic Processing Applications.
20. Hassler C, Boretius T, Stieglitz T (2011) Polymers for neural implants. *Journal of Polymer Science Part B Polymer Physics* 49: 18-33.
21. Ohsawa I, Inui K (2009) Use of tripolar electrodes for minimization of current spread in uncut peripheral nerve stimulation. *Neurosci Res* 64: 63-66.
22. Franssila S (2010) Introduction to Microfabrication. Introduction to Microfabrication (2nd edn), A John Wiley and sons Ltd, United Kingdom.
23. Cullinane JB (1990) User's evaluation of pin grid array sockets. *Connect Specif* 6: 39-44.
24. Yannas IV (2015) Tissue and Organ Regeneration in Adults. Springer. New York.
25. Yannas IV (2015) Tissue and Organ Regeneration in Adults. Springer. New York.
26. Borke RC, Curtis M, Ginsberg C (1993) Choline acetyltransferase and calcitonin gene-related peptide immunoreactivity in motoneurons after different types of nerve injury. *J Neurocytol* 22: 141-153.
27. Yuan Q, Su H, Chiu K, Lin ZX, Wu W (2014) Assessment of the rate of spinal motor axon regeneration by choline acetyltransferase immunohistochemistry following sciatic nerve crush injury in mice. *J Neurosurg* 120: 502-528.
28. Behan WM, Cossar DW, Madden HA, McKay IC (2002) Validation of a simple, rapid, and economical technique for distinguishing type 1 and 2 fibres in fixed and frozen skeletal muscle. *J Clin Pathol* 55: 375-380.
29. Kumar V, Abbas A, Nelson Fausto JA (2010) Robbins and Cotran Pathologic Basis of Disease. Elsevier, USA.
30. Navarro X, Valderrama E, Stieglitz T, Schüttler M (2001) Selective fascicular stimulation of the rat sciatic nerve with multipolar polyimide cuff electrodes. *Restor Neurol Neurosci* 18: 9-21.
31. Chamberlain LJ, Yannas IV, Hsu HB, Strichartz G, Spector M (1998) Collagen-GAG substrate enhances the quality of nerve regeneration through collagen tubes up to level of autograft. *Exp Neurol* 154: 315-329.
32. Lowrie MB, Krishnan S, Vrbová G (1987) Permanent changes in muscle and motoneurons induced by nerve injury during a critical period of development of the rat. *Brain Res* 428: 91-101.
33. Lago N, Navarro X (2006) Correlation between target reinnervation and distribution of motor axons in the injured rat sciatic nerve. *J Neurotrauma* 23: 227-240.
34. da Silva CF, Madison R, Dikkes P, Chiu TH, Sidman RL (1985) An in vivo model to quantify motor and sensory peripheral nerve regeneration using bioresorbable nerve guide tubes. *Brain Res* 342: 307-315.
35. Moldovan M, Sørensen J, Krarup C (2006) Comparison of the fastest regenerating motor and sensory myelinated axons in the same peripheral nerve. *Brain* 129: 2471-2483.
36. Lago N, Ceballos D, Rodríguez FJ, Stieglitz T, Navarro X (2005) Long term assessment of axonal regeneration through polyimide regenerative electrodes to interface the peripheral nerve. *Biomaterials* 26: 2021-2031.
37. Stieglitz T, Beutel H, Schuettler M, Meyer JU (2000) Micromachined, Polyimide-Based Devices for Flexible Neural Interfaces. *Biomed Microdevices* 2: 283-294.

This article was originally published in a special issue, entitled: "**Neuroscience and Rehabilitation**", Edited by Fuminari Kaneko, Sapporo Medical University, Japan and Tadayoshi Asaka, Hokkaido University, Japan